JOURNAL OF APPLIED PHYSICS **112**, 044313 (2012)

Thermoelectric properties of $Ba_8Ga_{16}Ge_{30}$ with TiO_2 nanoinclusions

R. Heijl,[1] D. Cederkrantz,[1] M. Nygren,[2] and A. E. C. Palmqvist[1]
[1]*Department of Chemical and Biological Engineering, Chalmers University of Technology, SE-41296 Göteborg, Sweden*
[2]*Department of Materials and Environmental Chemistry, Arrhenius Laboratory, Stockholm University, SE-10691 Stockholm, Sweden*

(Received 11 May 2012; accepted 20 July 2012; published online 30 August 2012)

The effects on thermal and electrical properties of adding small amounts of TiO_2 nanoinclusions to bulk $Ba_8Ga_{16}Ge_{30}$ clathrate have been investigated. The thermal properties were analysed using the transient plane source technique and the analysis showed a significant decrease in thermal conductivity as the volume fraction of TiO_2 increased from 0 vol. % to 1.2 vol. %. The introduction of TiO_2 nanoparticles caused a shift in the peak value of the Seebeck coefficient towards lower temperatures. The maximum value of the Seebeck coefficient was, however, only little affected. The introduction of TiO_2 nanoparticles into the bulk $Ba_8Ga_{16}Ge_{30}$ resulted in an increased electrical resistivity of the sample, thus simultaneously reducing the charge carrier contribution to the thermal conductivity, partly explaining the decrease in total thermal conductivity. Due to the large increase in resistivity of the samples, ZT was only somewhat improved for the material with 0.4 vol. % TiO_2 while the ZT values of the other materials were lower than for the reference $Ba_8Ga_{16}Ge_{30}$ material without TiO_2 nanoparticles. The combined results are consistent with a scenario where the nanoparticle introduction causes a light doping of the semiconductor matrix and an increased concentration of phonon scattering centres. © *2012 American Institute of Physics*. [http://dx.doi.org/10.1063/1.4748152]

INTRODUCTION

The conversion of chemically stored energy into useful mechanical or electrical energy has been at the centre of attention for scientists since the start of the industrial revolution in the 19th century. Today the focus is put on a more efficient use of the available fuel. This is largely due to increasing energy prices and global environmental concerns. There is no single answer to these challenges, but a small part of a more energy-efficient and environmentally friendly future society could be the use of thermoelectric materials for waste heat recovery. Thermoelectric materials can convert a temperature gradient into electrical current through a non-destructive solid-state process. For long these materials have had too low conversion rates relative to their cost to be considered for large scale commercial applications and have thus been used only in very specialized applications, e.g., in the space industry where functionality and reliability are most important. Today the situation is changing and thermoelectric generators are becoming part of the plans for the future of, e.g., the automotive industry. Since the mid 1990s, when Slack presented the concept of the phonon glass electron crystal (PGEC)[1] and Dresselhaus *et al.* showed that reducing the dimensions of thermoelectric materials has great potential to vastly improve their thermoelectric properties,[2,3] great progress has been made in the field. The potential of a thermoelectric material is governed by its Seebeck coefficient (S), electrical conductivity (σ), and thermal conductivity (κ). These properties can be combined in a dimensionless figure-of-merit, $ZT = TS^2\sigma/\kappa$, where T is the absolute temperature. The larger ZT is, the more efficient the material. Therefore an efficient thermoelectric material should have a large Seebeck, high electrical conductivity and low thermal conductivity. This, of course, is not easily achieved since all these properties are interrelated. Large efforts are made to find paths around these interrelations, e.g., by selectively lowering the phonon part of the thermal conduction without affecting the electrical conductivity. This can be done using complex crystal structures or by creating heterostructures, achieved, e.g., by introducing nanoparticles of one material into the bulk matrix of another thermoelectric material to reduce the phonon mean free path in the composite material.[4] An additional effect of introducing nanoparticles has been suggested to increase the Seebeck coefficient by filtering low energy electrons through a mechanism of bending the band structure at the interface between the nanoinclusions and the bulk phase and thus creating an energy barrier which only electrons with high enough energy can surpass.[5] The efficiency of this concept is currently under debate and more studies of such systems are needed.[6–8]

It has been reported that introduction of TiO_2 nanoparticles has a positive effect on the ZT value of $Ba_{0.22}Co_4Sb_{12}$ filled skutterudites,[9] and it is therefore of interest to investigate if a similar effect can be obtained for other high performing thermoelectric materials. The $Ba_8Ga_{16}Ge_{30}$ clathrate has received much interest as a high performance n-type thermoelectric material with the highest reported $ZT = 1.35$ at 900 K.[10–18] In this paper, the effects on the thermoelectric properties of $Ba_8Ga_{16}Ge_{30}$ clathrate achieved by the addition of TiO_2 nanoparticles are evaluated.

EXPERIMENTAL METHODS

Preparation of materials

A batch of 30 g of $Ba_8Ga_{16}Ge_{30}$ clathrate was prepared from high purity elements; Ba, Ga, and Ge (Sigma-Aldrich)

by direct solid state reaction at high temperature. To achieve high phase purity, a 2.5 wt. % of excess Ba was added as proposed by Saramat *et al.*[14] The elements were mixed in a glove box with a high purity argon environment and placed in alumina crucibles, which were subsequently placed in a sealed quartz tube. The quartz tube was first evacuated and then placed in a furnace (Thermolyne 21100 tube furnace with Eurotherm controller). The reaction vessel was first heated to a temperature of 1050 °C to ensure melting and the temperature was then lowered to 963 °C for crystal growth and kept there for 38 h, similar to a previously described method.[19] The vessel was then cooled (100 °C/h) to room temperature. The prepared material was removed from the crucible and ground to a fine powder using a Retsch MM400 mixer mill.

Three materials were prepared by mixing parts of the $Ba_8Ga_{16}Ge_{30}$ clathrate powder with different amounts of TiO_2 nanoparticles, amounting to 0.4 vol. %, 0.8 vol. %, and 1.2 vol. % of TiO_2, respectively. The TiO_2 nanoparticles, from Sigma-Aldrich (prod. #637262), had the rutile structure and a broad particle size distribution with an average diameter below 100 nm. The particles were mixed with the $Ba_8Ga_{16}Ge_{30}$ powder, using the mixer mill, with the purpose of crushing possible agglomerates of TiO_2 particles and dispersing them evenly in the clathrate powder matrix. The powders were then compacted using the spark plasma sintering (SPS) technique (Dr. Sinter 2050, SPS Syntex Inc., Japan) placing the powder in graphite dies and applying a temperature of 700 °C and a pressure of 100 MPa. The sintered bodies were cylinders of 12 mm diameter and 6–7 mm thickness. Each cylinder was cut in half so that two discs of 2–3 mm thickness each were obtained from each material and these pairs were subsequently used for thermal conductivity measurements by sandwiching the transient plane source (TPS)-sensor between them. After the thermal conductivity measurements, the discs were cut into rectangular bars of $10 \times 3 \times 3$ mm^3 on which measurements of Seebeck coefficient and electrical resistivity were performed.

Characterization of materials

The milled clathrate powder was analysed with x-ray diffraction to confirm crystal structure and phase purity using a Bruker XRD D8 Advance instrument. Data were collected within 2θ angles 20°–60° using Cu K_α radiation ($\lambda = 1.542$ Å) and uniform step size with a scanning time of 15 min. Analysis was also made on the sintered bodies to assess possible phase changes that might occur during sintering. For this measurement, a scanning time of 20 min was used.

The thermal conductivity (κ) of the sintered bodies was measured with a Hot Disk TPS 2500 S instrument. This is an instrument that uses the TPS technique.[20] The instrument uses a sensor made up of a double spiral of a conducting material connected to a highly sensitive voltmeter. The spiral acts as both sensor and heater. A constant current is sent through the spiral during the measurement, which raises the sensor temperature by a few degrees. The heat then dissipates into the sample and from the resulting temperature transient, monitored by the sensor, the thermal conductivity is calculated. The temperature of the sensor is measured by monitoring its resistance and relating it to the temperature through the temperature coefficient of resistance (TCR). The sensor has the shape of a very thin disc, with the metal double spiral protected on each side by a thin electrically insulating layer, in this case mica, and is sandwiched tightly between the two discs of the sample specimen. A particular limitation of the current version of the sensor is caused by the use of nickel in the double spiral. Nickel exhibits a change in its electrical properties in the vicinity of its Curie temperature that occurs at 358 °C around which measurements do not give physically meaningful values between 300 and 420 °C, as described elsewhere.[21] Measurements were performed at temperatures ranging from 100 to 650 °C and were repeated 5 times at each temperature. The results presented are averages of the five measurements at the respective temperature. All measurements were conducted under helium atmosphere.

The Seebeck coefficient (S) and the electrical resistivity ($1/\sigma$) of the sintered bodies were measured using an ULVAC ZEM-3 instrument. The measurements were performed between 100 and 650 °C in low pressure He atmosphere. The resistivity is measured with a standard 4-point probe method by sending a step current through the sample rod and at the same time using two probes to measure the voltage difference along the length of the rod. This way the resistance of the sample can be calculated and with known sample dimensions the electrical resistivity is obtained. The Seebeck coefficient is acquired by heating one end of the sample rod, creating a temperature gradient, and then measuring the generated potential between the probes. For each measurement temperature, three different temperature gradients were used to minimize the measurement error. The measurements were made during both increasing and decreasing temperature ramps to assess the presence of possible hysteresis effects.

The electrical property measurements were complemented by Hall measurements at 300 K and 400 K using a physical property measurement system (PPMS), from Quantum Design, employing the ACT module with horizontal rotator. For these measurements, a five wire setup and a magnetic field direction at both 0° and 180° were employed.

RESULTS AND DISCUSSION

Structural characterization

The XRD diffractogram of the prepared clathrate powder matched very well that previously reported.[22] The concentration of the commonly observed germanium impurity phase was very low. After sintering, some of the samples had small cracks and were somewhat brittle. The XRD analysis of the sintered samples (see Fig. 1) showed the appearance of small peaks due to germanium formed during the sintering process. The magnitude of these peaks increases with increasing TiO_2 content. The very small addition of TiO_2, in the combination with its small particle size, made it not possible to detect the TiO_2 phase with the XRD instrument used and possible decomposition products due to the sintering could not be discerned either.

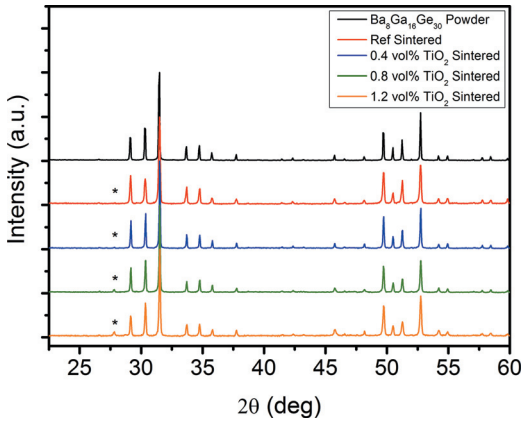

FIG. 1. X-ray diffractograms of the $Ba_8Ga_{16}Ge_{30}$ powder used for making all of the composites, the sintered $Ba_8Ga_{16}Ge_{30}$ reference material, and all of the sintered $Ba_8Ga_{16}Ge_{30}$ materials with TiO_2 included. The asterisk marks the germanium (111) peak found as an impurity in some of the sintered materials.

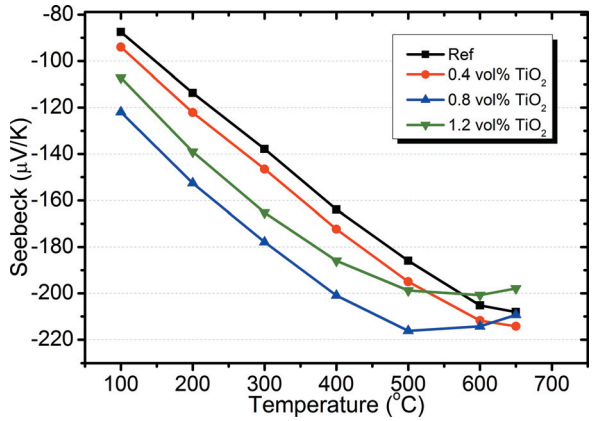

FIG. 3. Seebeck coefficient of $Ba_8Ga_{16}Ge_{30}$ materials with different amounts of TiO_2 nanoparticles. The sample labelled Ref is the $Ba_8Ga_{16}Ge_{30}$ material without TiO_2 included.

Electrical properties

The electrical resistivity of the studied materials was found to greatly increase with the concentration of added TiO_2 nanoparticles as shown in Fig. 2. This is expected, partly because the electrical conductivity of TiO_2 is very poor and partly as a result of an increased number of scattering interfaces. The reference sample free from TiO_2 and the 0.4 vol. % TiO_2 sample both show the typical behaviour of heavily doped semiconductors where the intrinsic transition appears to be present somewhat above 650 °C. The materials with higher amounts of TiO_2 show a more complex semiconducting behaviour, having a local maximum in resistivity at 500 °C, indicating that the intrinsic transition occurs at a lower temperature compared to the reference sample and the 0.4 vol. % sample. The lower intrinsic transition temperature in turn points toward a lower charge carrier concentration consistent with the reduced overall electrical conductivity observed. Fig. 3 shows the measured values of the Seebeck coefficients of the studied materials. The material with 0.4 vol. % TiO_2 shows a slight increase in absolute values of the Seebeck coefficient compared to the reference clathrate material without TiO_2, in a similar trend as that observed for the resistivity and with apparent maxima somewhat above 650 °C. The two materials with higher TiO_2 content show maxima in Seebeck coefficient at 500 °C, the same temperature as their local maxima in resistivity, consistent with a reduction in the concentration of charge carriers as discussed above. The results of the Hall measurements performed at 27 °C and 127 °C have been converted to charge carrier concentrations and are presented in Fig. 4. From these measurements, it can be seen that the addition of TiO_2 to the $Ba_8Ga_{16}Ge_{30}$ clathrate has a complex effect on the charge carrier concentration where the material with 0.4 vol. % TiO_2 shows a higher carrier concentration than the reference whereas the materials with higher amounts of TiO_2 show lower carrier concentrations. These results are in general accordance with the observed effects on the electrical resistivity and the Seebeck coefficient and explains why the resistivity is only slightly increased for the 0.4 vol. % sample while significantly more so for the samples with higher concentrations of TiO_2. Judging from the similar behaviour of the reference sample and the 0.4 vol. % TiO_2 sample, and the samples with 0.8 and 1.2 vol. % TiO_2, respectively, there seems to be a threshold somewhere in the vicinity of 0.4 vol. % TiO_2, above which the combined effects of additional TiO_2 particles in the $Ba_8Ga_{16}Ge_{30}$ matrix on the charge

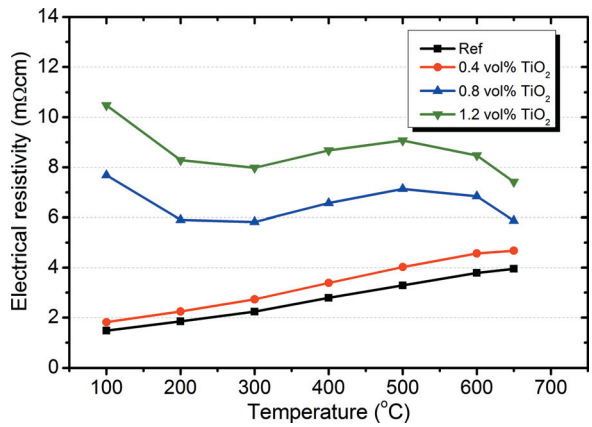

FIG. 2. Electrical resistivity of $Ba_8Ga_{16}Ge_{30}$ materials with different amounts of TiO_2 nanoparticles. The sample labelled Ref is the $Ba_8Ga_{16}Ge_{30}$ material without TiO_2 included.

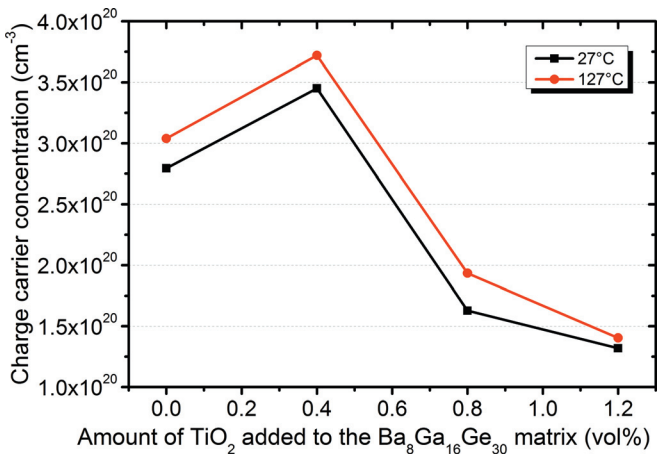

FIG. 4. Experimental charge carrier concentrations for all $Ba_8Ga_{16}Ge_{30}$ samples at 27 °C and 127 °C, as a function of TiO_2 content in the matrix.

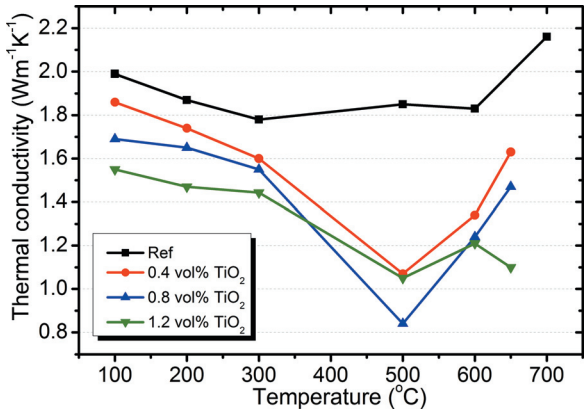

FIG. 5. The thermal conductivity of $Ba_8Ga_{16}Ge_{30}$ materials with different amounts of TiO_2 nanoparticles. The sample labelled Ref is the $Ba_8Ga_{16}Ge_{30}$ material without TiO_2 included.

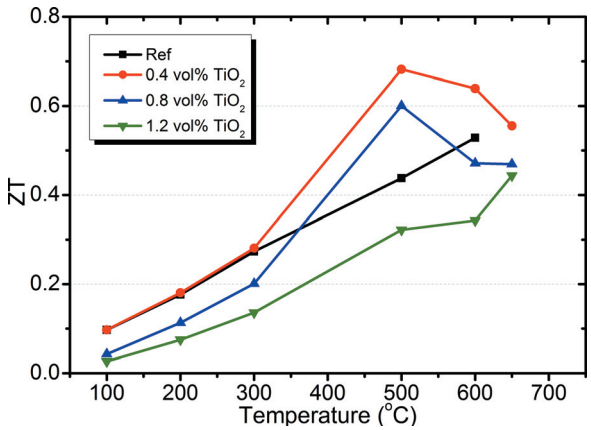

FIG. 7. The figure of merit, ZT, of $Ba_8Ga_{16}Ge_{30}$ materials with different amounts of TiO_2 nanoparticles. The sample labelled Ref is the $Ba_8Ga_{16}Ge_{30}$ material without TiO_2 included.

carrier concentration and mobility affect the material properties unfavourably, i.e., the electrical conductivity is greatly reduced while the thermopower has reached an optimum after which it slowly declines. The high carrier concentration found for the 0.4 vol. % material is believed to be due to a partial reduction of the TiO_2 that results in doping of the clathrate, with Ti donating electrons to the material in a similar fashion to that observed for TiO_2 in Mg_2Si.[23] Presumably, it is not possible to reduce the larger quantities of TiO_2 which is why those materials have lower carrier concentrations, proposing that TiO_2 in excess of the threshold has a reversed effect on the doping level.

Thermal conductivity

In Fig. 5, the thermal conductivity of the four materials is presented showing a general trend of decreasing thermal conductivity with increasing amount of TiO_2 inclusions added, as expected. A minimum in thermal conductivity was found around 500 °C for all samples except the pure $Ba_8Ga_{16}Ge_{30}$ reference. The accuracy of the measurements is somewhat lower at higher temperatures, but it is still clear that the addition of TiO_2 nanoparticles effectively reduces the thermal conductivity of the material. Using the Wiedemann-Franz law, the relative contributions of charge carrier and lattice parts to the thermal conductivity can be obtained as presented in Fig. 6. It can thus be seen that the largest influence on the thermal conductivity comes from the reduced electrical conductivity. However, the change in thermal conductivity cannot be explained exclusively by the reduced electrical conductivity. Especially, the minimum in thermal conductivity of the 0.4 vol. % sample that appears at 500 °C has no corresponding minimum in the electrical conductivity. This suggests instead that the TiO_2 nanoparticles provide some additional phonon scattering mechanism that causes the dip in thermal conductivity at 500 °C.

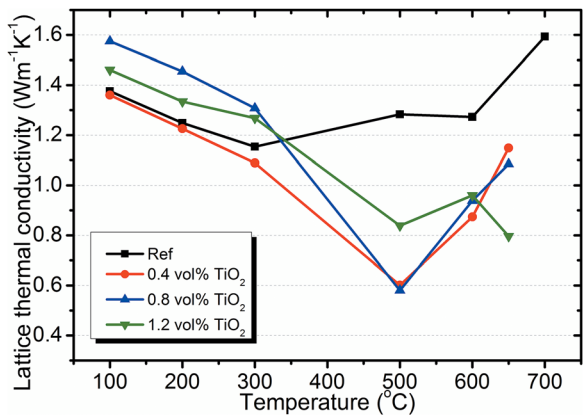

FIG. 6. Lattice thermal conductivity of $Ba_8Ga_{16}Ge_{30}$ materials with different amounts of TiO_2 nanoparticles, as calculated using Wiedemann-Franz law. The sample labelled Ref is the $Ba_8Ga_{16}Ge_{30}$ material without TiO_2 included.

Figure of merit, ZT

When combining the measured data of electrical and thermal properties of the studied materials into the figure-of-merit, as presented in Fig. 7, it can be seen that the material with 0.4 vol. % TiO_2 added yielded the highest ZT within the temperature range of 300–650 °C. This is mainly due to the reduced thermal conductivity since the effects of reduced electrical conductivity and improved Seebeck values more or less cancel each other. It is furthermore found that a very high amount of TiO_2 raised the electrical resistivity of the samples to such high levels that the decrease in thermal conductivity and somewhat improved thermopower were not sufficient to improve the overall thermoelectric efficiency over that of the reference material. It is also interesting to note that the best sample has a peak ZT value at 500 °C, whereas the reference sample appears to have its peak ZT above 650 °C. This decrease in ZT optimum is due to the mixed mechanisms causing the reduction in thermal conductivity.

CONCLUSIONS

In summary, the method evaluated has produced materials with lower thermal conductivity than the reference. The nanoinclusions that were introduced into the $Ba_8Ga_{16}Ge_{30}$ matrix tend to mainly affect the electronic transport properties of the material, which is believed to be the main reason

for the reduction in thermal conductivity. It was seen that the addition of TiO_2 can have different effects on the charge carrier concentration of the material, depending on the amount used. An apparent threshold around 0.4 vol. % TiO_2 was found, below which the charge carrier concentration increases with increasing TiO_2 addition, and above which it decreases. This suggests that there are at least two different opposing mechanisms that cause the TiO_2, and whatever products that might form during sintering, to alter the charge carrier concentration. These effects, together with grain boundary effects on charge carriers and phonons, result in improved ZT values upon addition of a small amount of TiO_2 nanoinclusions, in this case 0.4 vol. %, while a higher nanoparticle concentration worsen the ZT value. However, an important observation made in this study is that the combined change in electrical and thermal properties makes the maximum in ZT appear at lower temperature. In this way, the temperature for maximum ZT can be altered to better suit its application.

ACKNOWLEDGMENTS

The Swedish Foundation for Strategic Environmental Research, Mistra, is gratefully acknowledged for financial support through the E4 Mistra program. AECP acknowledges the Swedish Research Council (VR) for support through a Senior Researcher position.

[1]G. A. Slack, in *CRC Handbook of Thermoelectrics*, edited by D. M. Rowe (CRC LLC, Boca Raton, 1995), Chap. 34.
[2]M. S. Dresselhaus, G. Dresselhaus, X. Sun, Z. Zhang, S. B. Cronin, T. Koga, J. Y. Ying, and G. Chen, Microscale Thermophys. Eng. **3**, 89–100 (1999).
[3]L. D. Hicks and M. S. Dresselhaus, Phys. Rev. B **47**, 12727–12731 (1993).
[4]D. L. Medlin and G. J. Snyder, Curr. Opin. Colloid Interface Sci. **14**, 226–235 (2009).
[5]S. V. Faleev and F. Leonard, Phys. Rev. B **77**, 214304 (2008).
[6]J. M. O. Zide, D. Vashaee, Z. X. Bian, G. Zeng, J. E. Bowers, A. Shakouri, and A. C. Gossard, Phys. Rev. B **74**, 205335 (2006).
[7]N. Mingo, D. Hauser, N. P. Kobayashi, M. Plissonnier, and A. Shakouri, Nano Lett. **9**, 711–715 (2009).
[8]J. R. Szczech, J. M. Higgins, and S. Jin, J. Mater. Chem. **21**, 4037–4055 (2011).
[9]Z. Xiong, X. H. Chen, X. Y. Zhao, S. Q. Bai, X. Y. Huang, and L. D. Chen, Solid State Sci. **11**, 1612–1616 (2009).
[10]A. Saramat, G. Svensson, A. E. C. Palmqvist, C. Stiewe, E. Mueller, D. Platzek, S. G. K. Williams, D. M. Rowe, J. D. Bryan, and G. D. Stucky, J. Appl. Phys. **99**, 023708 (2006).
[11]E. S. Toberer, M. Christensen, B. B. Iversen, and G. J. Snyder, Phys. Rev. B **77**, 075203 (2008).
[12]H. Anno, M. Hokazono, M. Kawamura, J. Nagao, and K. Matsubara, in *Proceedings of the 21st International Conference on Thermoelectrics* (IEEE, 2002), pp. 77–80.
[13]M. Christensen, S. Johnsen, and B. B. Iversen, Dalton Trans. **39**, 978–992 (2010).
[14]A. Saramat, E. S. Toberer, A. F. May, and G. J. Snyder, J. Electron. Mater. **38**, 1423–1426 (2009).
[15]D. Cederkrantz, M. Nygren, and A. E. C. Palmqvist, J. Appl. Phys. **108**, 113711 (2010).
[16]M. Christensen, A. B. Abrahamsen, N. B. Christensen, F. Juranyi, N. H. Andersen, K. Lefmann, J. Andreasson, C. R. H. Bahl, and B. B. Iversen, Nature Mater. **7**, 811–815 (2008).
[17]H. Kleinke, Chem. Mater. **22**, 604–611 (2010).
[18]E. S. Toberer, A. F. May, and G. J. Snyder, Chem. Mater. **22**, 624–634 (2010).
[19]D. Cederkrantz, A. Saramat, G. J. Snyder, and A. E. C. Palmqvist, J. Appl. Phys. **106**, 074509 (2009).
[20]S. E. Gustafsson, Rev. Sci. Instrum. **62**, 797–804 (1991).
[21]D. Cederkrantz, M. Søndergaard, M. Christensen, B. B. Iversen, and A. E. C. Palmqvist, "A comparison between the laser flash method and the transient plane source technique for bulk thermal conductivity measurements from a thermoelectric materials perspective" (submitted).
[22]A. Bentien, E. Nishibori, S. Paschen, and B. B. Iversen, Phys. Rev. B **71**, 144107 (2005).
[23]D. Cederkrantz, N. Farahi, K. A. Borup, B. B. Iversen, M. Nygren, and A. E. C. Palmqvist, J. Appl. Phys. **111**, 023701 (2012).